

# Cellulose Nanocrystal Aqueous Colloidal Suspensions: Evidence of Density Inversion at the Isotropic-Liquid Crystal Phase Transition

Rafaela R. da Rosa, Pedro E. S. Silva, Diogo V. Saraiva, Anant Kumar, António P. Mendes de Sousa, Pedro Sebastião, Susete N. Fernandes, and Maria Helena Godinho\*

The colloidal suspensions of aqueous cellulose nanocrystals (CNCs) are known to form liquid crystalline (LC) systems above certain critical concentrations. From an isotropic phase, tactoid formation, growth, and sedimentation have been determined as the genesis of a high-density cholesteric phase, which, after drying, originates solid iridescent films. Herein, the coexistence of a liquid crystal upper phase and an isotropic bottom phase in CNC aqueous suspensions at the isotropic–nematic phase separation is reported. Furthermore, isotropic spindle-like domains are observed in the low-density LC phase and high-density LC phases are also prepared. The CNCs isolated from the low- and high-density LC phases are found to have similar average lengths, diameters, and surface charges. The existence of an LC low-density phase is explained by the presence of air dissolved in the water present within the CNCs. The air dissolves out when the water solidifies into ice and remains within the CNCs. The self-adjustment of the cellulose chain conformation enables the entrapment of air within the CNCs and CNC buoyancy in aqueous suspensions.

## 1. Introduction

Rod-like colloidal suspensions are known to exhibit a transition from a disordered isotropic (I) phase to an ordered liquid crystalline (LC) phase.<sup>[1–3]</sup> As noted by Onsager, this transition can be explained by entropic arguments.<sup>[1]</sup> The nematic phase is stable because at higher particle concentrations, the orientational entropy loss associated with particle alignment is balanced by the gain in the configurational entropy. It has been reported that cellulose nanocrystals (CNCs) isolated through sulfuric acid hydrolysis form colloidal suspensions in water,<sup>[4]</sup> and above a certain critical concentration, form birefringent domains. The critical concentration and the stability of the anisotropic phase depend upon the dimensions, size, polydispersity, and surface charge of the nanocrystals. Cellulose anisotropic structures have also been found in vivo. In 1976,<sup>[5]</sup> the existence of helicoidal cellulose architectures in *Chara vulgaris* cell walls was reported. More recently, helicoidal structures have been found responsible for the structural colors in certain plants.<sup>[6,7]</sup> These helicoidal structures are similar to those of cholesteric liquid crystals formed by pseudo-nematic layers twisted around an axis (optical axis) normal to the direction defined by the director (**n**) in each layer. While all the molecules are oriented in the same average direction in each plane, this direction is shifted by a few degrees from plane-to-plane, forming a helix.<sup>[8,9]</sup> Cholesteric phases are characterized by the pitch (*P*) and handedness. The pitch, estimated as the distance necessary for the director to rotate by 360°, is a function of the temperature and concentration. The nematic chiral structure shows high-optical activity when viewed along the optical axis. As cholesteric liquid crystals self-assemble spontaneously, it has been suggested that a similar mechanism may be at work in the morphogenesis formation of the helicoidal structures found in biological systems.<sup>[10]</sup> Later, in 1992, it was reported that negatively charged CNCs, obtained through acid hydrolysis in sulfuric acid, could form chiral nematic ordered phases in water.<sup>[11]</sup> The stability of the suspensions was highly sensitive to the presence of sulfate ester groups on the CNC surface.<sup>[12–14]</sup> The stability of the CNC suspensions was also found to be affected by other factors such


tures have also been found in vivo. In 1976,<sup>[5]</sup> the existence of helicoidal cellulose architectures in *Chara vulgaris* cell walls was reported. More recently, helicoidal structures have been found responsible for the structural colors in certain plants.<sup>[6,7]</sup> These helicoidal structures are similar to those of cholesteric liquid crystals formed by pseudo-nematic layers twisted around an axis (optical axis) normal to the direction defined by the director (**n**) in each layer. While all the molecules are oriented in the same average direction in each plane, this direction is shifted by a few degrees from plane-to-plane, forming a helix.<sup>[8,9]</sup> Cholesteric phases are characterized by the pitch (*P*) and handedness. The pitch, estimated as the distance necessary for the director to rotate by 360°, is a function of the temperature and concentration. The nematic chiral structure shows high-optical activity when viewed along the optical axis. As cholesteric liquid crystals self-assemble spontaneously, it has been suggested that a similar mechanism may be at work in the morphogenesis formation of the helicoidal structures found in biological systems.<sup>[10]</sup> Later, in 1992, it was reported that negatively charged CNCs, obtained through acid hydrolysis in sulfuric acid, could form chiral nematic ordered phases in water.<sup>[11]</sup> The stability of the suspensions was highly sensitive to the presence of sulfate ester groups on the CNC surface.<sup>[12–14]</sup> The stability of the CNC suspensions was also found to be affected by other factors such

R. R. da Rosa, P. E. S. Silva, D. V. Saraiva, S. N. Fernandes, M. H. Godinho  
i3N/CENIMAT

Department of Materials Science  
NOVA School of Science and Technology  
NOVA University Lisbon  
Campus de Caparica, Caparica 2829-516, Portugal  
E-mail: mhg@fct.unl.pt

A. Kumar, P. Sebastião  
Centro de Física e Engenharia de Materiais Avançados  
Departamento de Física  
Instituto Superior Técnico  
Universidade de Lisboa  
Av. Rovisco Pais, Lisbon 1049-001, Portugal

A. P. M. de Sousa  
RAIZ – Forest and Paper Research Institute  
Quinta de S. Francisco, Rua José Estevão (EN 230-1)  
Eixo 3800-783, Portugal

 The ORCID identification number(s) for the author(s) of this article can be found under <https://doi.org/10.1002/adma.202108227>.

© 2022 The Authors. Advanced Materials published by Wiley-VCH GmbH. This is an open access article under the terms of the Creative Commons Attribution License, which permits use, distribution and reproduction in any medium, provided the original work is properly cited.

DOI: 10.1002/adma.202108227

as freeze–thaw (FT), which was reported to generate aggregation and gel formation in CNC suspensions.<sup>[15]</sup> While CNCs hydrolyzed in sulfuric or phosphoric acid were reported to form chiral nematic phases, those obtained through hydrochloric acid hydrolysis did not form colloidal cholesteric phases.<sup>[16,17]</sup> Since then, several reports on controlling the optical characteristics of solid iridescent films that can be produced from charged CNCs (with sulfate esters) colloidal cholesteric suspensions after solvent evaporation have been published.<sup>[18]</sup>

Separation is known to occur between the isotropic and anisotropic phases in lyotropic colloidal CNC suspensions via the formation of LC microdroplets (tactoids) formed in the isotropic phase. Subsequently, the tactoids coalesce, and due to gravity, deposits at the bottom of the samples, forming a high-density LC phase.<sup>[19]</sup> The formation of anisotropic tactoids from the isotropic phase requires particles with a higher aspect ratio (length ( $L$ )/diameter ( $D$ ) ( $L/D$ )) than that of the particles existing in the isotropic phase. The kinetic transfer of particles with high  $L/D$  values from the isotropic to anisotropic phase causes the nucleation of tactoids.<sup>[20]</sup> To the best of our knowledge, the formation of an LC phase above an isotropic phase in CNC aqueous colloidal suspensions at the isotropic–nematic phase separation has not yet been reported. Onsager<sup>[1]</sup> theory predicts the values of the critical concentration for phase separation based on the values of  $L$  and  $D$  of the particles. Under the coexistence of the isotropic ( $\phi_i$ ) and liquid crystalline ( $\phi_{LC}$ ) phases are given by  $\phi_i = 3.3 D/L$  and  $\phi_{LC} = 4.2 D/L$ , according to Onsager and other authors.<sup>[1,21,22]</sup> In addition, other colloidal lyotropic suspensions, such as those of vanadium pentoxide sols,<sup>[23]</sup> tobacco mosaic viruses,<sup>[24]</sup> and iron oxyhydroxide nanorods,<sup>[25]</sup> have been described in literature.

Another type of tactoids that are less addressed in colloidal suspensions is atactoids or negative tactoids. Atactoids consist of isotropic microdomains that develop in a continuous LC phase. They have been observed in colloidal lyotropic LC systems formed by long-filaments as in vanadium pentoxide sols<sup>[23]</sup> and in the suspensions of actin filaments (F-actin)<sup>[26]</sup> but have not been reported in CNC lyotropic systems. Dried samples prepared from  $V_2O_5$  aqueous dispersions revealed the presence of elliptical holes, similar to the atactoids present in colloidal suspensions.<sup>[23]</sup>

The colloidal suspensions of anisometric particles can display unexpected results, as those described for polydisperse platelets.<sup>[27]</sup> It has been reported that at the isotropic–nematic coexistence region, the density of the nematic phase can become lower than that of the isotropic phase.<sup>[27,28]</sup> The observed density inversion is mainly attributed to the highly asymmetric size distribution of the particle thickness.<sup>[27]</sup>

In this study, we demonstrate the development of a low-density nematic phase at the isotropic–nematic transition in CNC lyotropic colloidal aqueous suspensions. The CNCs are isolated through acid hydrolysis from different sources and under different conditions, according to literature.<sup>[29]</sup> However, after acid hydrolysis and before dialysis, the CNC suspensions are freeze–thawed, promoting their aggregation. The low-density LC phase is obtained from never-dried bleached *eucalyptus* kraft pulp (BEKP). Moreover, we show the existence of isotropic domains decorating the low-density LC phase. Phase diagrams

and polarized optical microscopy (POM) images of the LC suspensions are obtained.  $^1H$  NMR relaxometry is used to investigate the water dynamics in the high- and low-density LC CNC suspensions. The CNCs are characterized using atomic force microscopy (AFM), X-ray diffraction (XRD), and elemental analysis, while the solid films are characterized using IR spectroscopy, scanning electron microscopy (SEM), X-ray photoelectron spectroscopy (XPS), and wettability measurements.

We demonstrate that the presence of water in the fibers before extracting the CNCs and freeze–thawing the diluted suspensions after acid hydrolysis is crucial for the observed anomalous behavior.

## 2. Results

### 2.1. Preparation of CNCs and CNC Aqueous Colloidal Suspensions

CNC aqueous colloidal suspensions have been described as highly polydisperse rod-like systems. Particle populations with different lengths were obtained upon fractionation.<sup>[16]</sup> These suspensions exhibit isotropic–nematic phase separation over a wide range of rod concentrations, with an isotropic phase above a high-density nematic phase. Recently, the fractionation of CNC suspensions into rods of different lengths ( $L$ ) and identical diameters ( $D$ )<sup>[30]</sup> has been reported. Particles with high-aspect ratios ( $L/D$ ) form LC phases according to the Onsager theory.<sup>[1,21,22]</sup>

In this study, CNCs were isolated through hydrolysis in sulfuric acid, from different sources. The synthesis procedure was adapted from a previously described protocol for CNC preparation using concentrated sulfuric acid to promote the hydrolysis and esterification of cellulose<sup>[11,31]</sup> (further details can be found in the Experimental Section and the Supporting Information).

It is worth nothing that after acid hydrolysis and before dialysis, the CNC suspensions were freeze–thawed, which has not been previously reported as part of the CNC production process.

The following were used as the starting material for CNC preparation: never-dried BEKP (29% w/w water content) (sample (i)); dried BEKP (sample (ii)); re-hydrated BEKP (29% w/w water content) (sample (iii)); wet cotton (35% w/w of water) (sample (iv)). The pulp and starting cellulose samples comprised long cellulose fibrils (average length in the order of 700  $\mu m$  and diameter of 14  $\mu m$ ), from which CNCs can be readily isolated through acid hydrolysis.

### 2.2. CNC Aqueous Colloidal Suspensions

#### 2.2.1. Macroscopic Qualitative Observations

After dialysis, the CNC suspensions were placed in ultrapure water, and different CNC concentrations were prepared from samples: i) (CNCi), ii) (CNCii), iii) (CNCiii), and iv) (CNCiv). The suspensions obtained from CNCi and CNCii after a month are shown in **Figure 1a,b**, respectively. Surprisingly, the CNCi suspensions show a low-density LC phase (CNCiLC) in

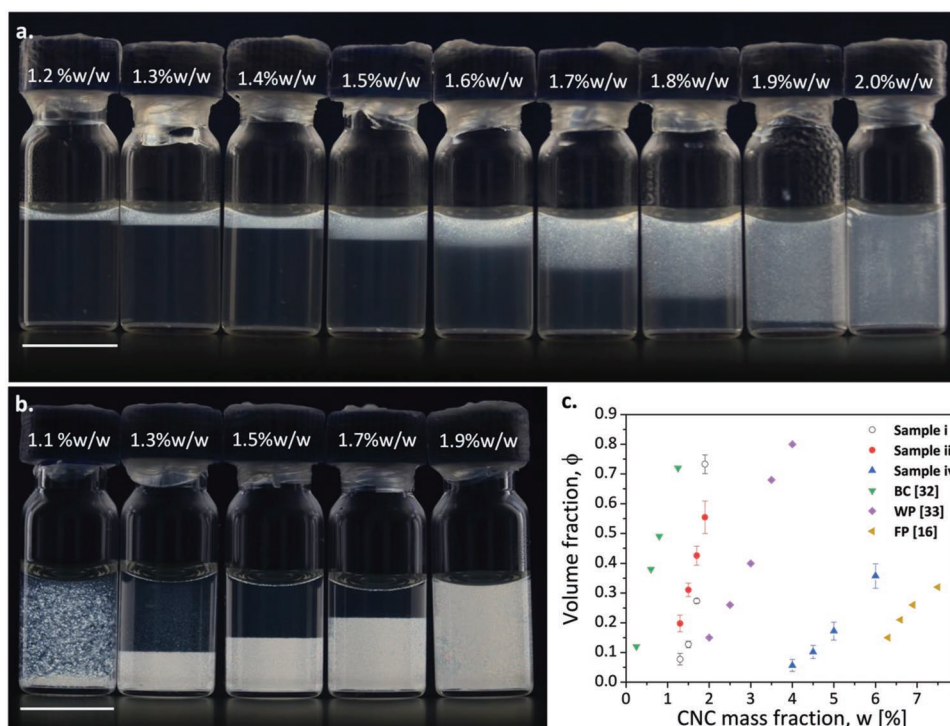


**Figure 1.** Phase inversion in CNC colloidal water suspensions. a,b) Phase separation of the CNCs prepared from CNCi (a) and CNCii (b) aqueous suspensions, respectively, observed between crossed polarizers. In the (a) series, the LC birefringent phase (CNCiLC) is atop the isotropic solution, whereas in the (b) series, the LC phase (CNCiiLC) accumulates at the bottom. The photos were captured a month after the colloidal suspensions were prepared. c) Relative volume of the anisotropic phase as a function of the total CNC concentration (% w/w) for the suspensions shown in (a) and (b) (after 2 months), CNCs from sample (i) and sample (ii), respectively, and the suspensions obtained from sample (iv), bacterial cellulose (BC),<sup>[32]</sup> wood pulp,<sup>[33]</sup> and filter paper (FP).<sup>[16]</sup> The open symbols indicate that the anisotropic phase is on top of the isotropic phase, whereas the closed symbols indicate the opposite. The error bars correspond to six measurements of each of the two series of vials prepared at the same concentration range for the series prepared from samples (i), (ii), and (iv). The scale bar in (a) and (b) is 1 cm.

addition to a high-density isotropic (I) phase (CNCiI); the suspensions from CNCii show a high-density LC phase (CNCiiLC) co-existing with an isotropic low-density phase (CNCiiI) as expected. The CNCiLC phase appears for a CNCi mass fraction of  $\approx 1.2\%$  w/w. The relative volume fraction increases monotonically from 0 to 1 with the mass fraction in the range of 1.2–2.0% w/w. Aqueous suspensions prepared from CNCii exhibit a completely different but expected behavior in accordance with previous reports. Macroscopic phase separation results in the separation of the high-density LC phase at CNC mass fractions ranging from 1.1 to 1.9% w/w, while the LC volume fraction increases from 0 to 1. Moreover, it is interesting to note that all aqueous suspensions prepared from CNCi present a clear separation between the isotropic and anisotropic phases (Figure 1a), while those prepared from CNCii with a mass fraction of 1.1% w/w show birefringent domains that require considerable time for sedimentation (Figure 1b). Furthermore, the mass fractions of the CNCi and CNCii samples in the LC and isotropic phases were determined. The CNCi and CNCii LC phases always have higher mass fractions compared to those of the isotropic phases. Surprisingly, the mass fraction of the low-density LC phase is higher than that of the high-density isotropic phase (Table S1, Supporting Information).

The phase diagrams of CNCi, CNCii, and CNCiv are depicted in Figure 1c, along with the values found in literature for CNCs

isolated from bacteria,<sup>[32]</sup> wood pulp,<sup>[33]</sup> and filter paper.<sup>[16]</sup> All samples show separation into an LC phase and an isotropic phase. The volume fraction of the LC phase increases with the CNC mass fraction, which differs between samples (Figures S2 and S3, Supporting Information). The critical CNC mass fraction for forming the LC phase is similar for the CNCi, CNCii, and never-dried wood pulp<sup>[33]</sup> samples, whereas it is lower for the CNCs obtained from bacteria<sup>[32]</sup> and higher for the CNCiv sample and the CNC suspensions from filter paper.<sup>[16]</sup>

Previous studies state that the critical concentration of the LC phase is expected to decrease for longer and thinner CNCs with high surface charges.<sup>[16,30,31]</sup> As the critical concentration for the appearance of the LC phase for CNCi, CNCii, and never-dried wood pulp<sup>[33]</sup> is similar according to literature, these samples should contain CNCs with similar average lengths, aspect ratios, and surface charges. The average  $L/D$  values for CNCi and CNCii are in the order of 40 (Table S2, Supporting Information), indicating that  $L$  is considerably larger than  $D$ , in accordance with the values reported in literature for the CNCs extracted from wood pulp.<sup>[16,18]</sup>

The presence of a high-density LC phase in the samples prepared from CNCii is very similar to the behavior described in literature for CNCs obtained from different wood pulp sources.<sup>[12,30,34]</sup> However, the behavior of the samples prepared from CNCi differs, despite having a critical concentration



similar to that of the suspensions prepared from CNCii and the CNC suspensions obtained from never-dried wood pulp.

To better characterize the development of the CNCiLC and CNCiiLC phases, one vial of each suspension with the same mass fraction (1.5% w/w) was observed with respect to time between crossed polarizers (Figure 2a,b, and Movie S1, Supporting Information).

Initially, the CNCi and CNCii suspensions appear birefringent. After 6 h, an isotropic phase starts to develop at the bottom in CNCi and at the top in the CNCii suspensions. The volume of the isotropic phase for both samples exponentially

increases with time (Figure 2c–e). Subsequently, at  $\approx 60$  h, a plateau regime is attained in both samples. This plateau in the CNCi suspension corresponds to a clear separation between the isotropic and LC phases; however, in the CNCii suspension, the plateau is not clear due to the presence of anisotropic domains (tactoids) that remain suspended in the isotropic phase (as observed in Figure 1b). The results obtained for suspension CNCii are in accordance with literature, where the sedimentation of tactoids can require months.<sup>[30]</sup>

Samples CNCi and CNCii (initial concentration of 1.5% w/w) were mixed with different ratios of CNCi ( $x_{\text{CNCi}} = \text{CNCi}/(\text{CNCi} + \text{CNCii})$ )

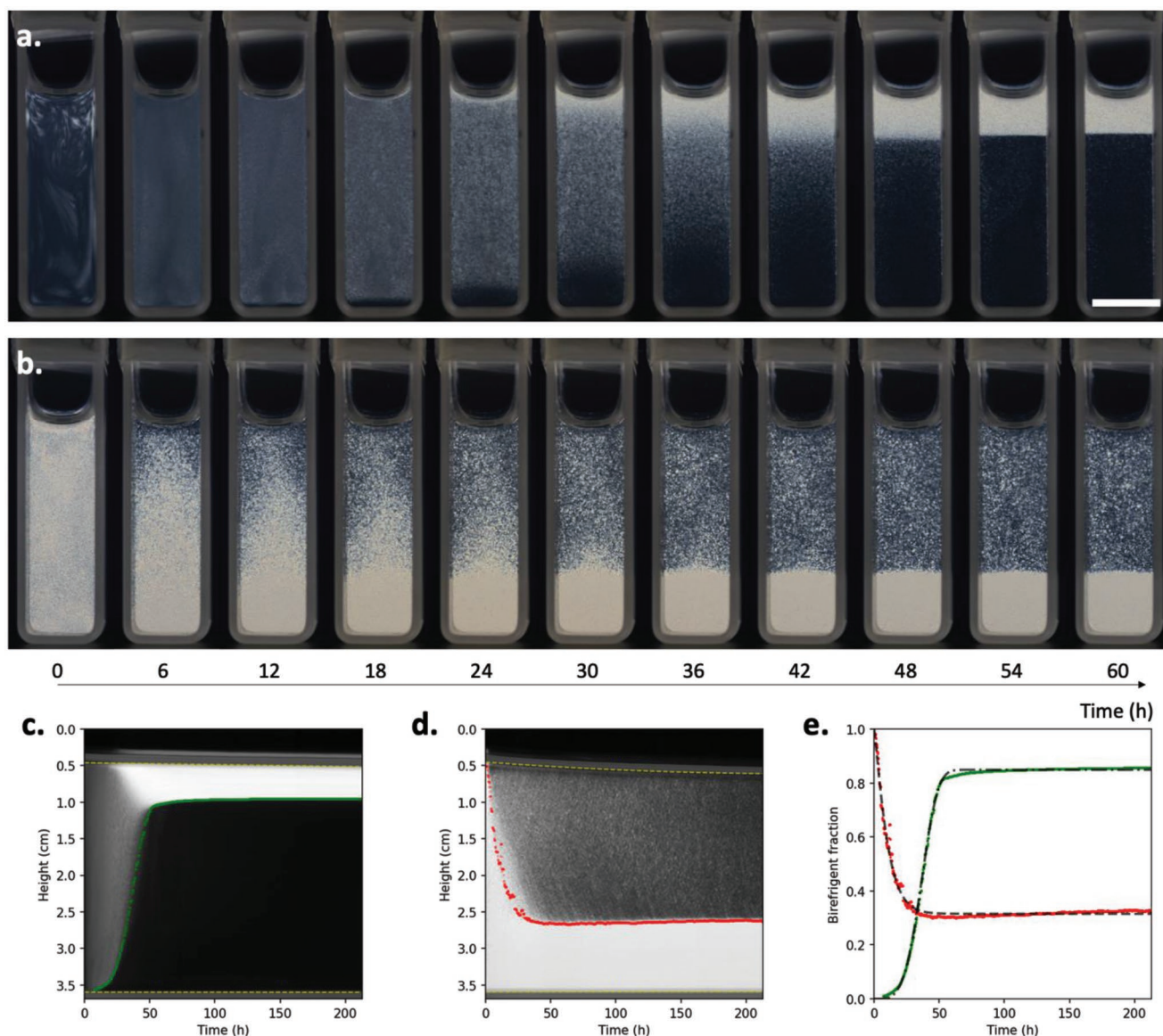


**Figure 2.** Time evolution of CNC aqueous suspensions. Vials showing the anisotropic–isotropic separation in CNCi suspensions (the anisotropic phase develops on top) (a) and CNCii suspensions (the anisotropic phase accumulates at the bottom) (b) for  $C = 1.5\%$  w/w CNC aqueous suspensions. The images are obtained between crossed polarizers and the scale bar is 1 cm. c,d) The particle separation profiles of the CNCi (c) and CNCii (d) suspensions. For each time step, the median value of the gray intensity across the vial was calculated. The white and black colors denote greater and lesser concentrations of anisotropic particles, respectively. The yellow dashed lines mark the boundaries of the vials and dots delimit two regions with different concentrations of anisotropic particles. e) Curve fitting of the points measured in (c) and (d). During the observed time-frame, both samples appear to follow exponential behavior.

+ CNCi) of 0.2, 0.4, 0.5, 0.6, and 0.8 (Figure S1, Supporting Information). All mixtures show a low-density LC phase that fully develops after 3–5 days. It is noteworthy that the isotropic/LC phase separation is sharper and occurs earlier for low fractions of CNCi than for low quantities of CNCii.

The CNCiii and CNCiv suspensions (Figure S3, Supporting Information) present a high-density LC phase as described for CNCii and well documented in literature.

### 2.2.2. Microscopic Textures

To further investigate the LC phases formed in the CNCi (Figure 3a) and CNCii (Figure 3b) suspensions, the anisotropic regions of both samples were collected from the vials, enclosed in flat capillaries, and observed using POM in the transmission mode, between crossed polarizers (Figure 3a1,b1–b3) and crossed polarizers and a lambda plate (Figure 3a2,b2–b4).

The LC texture of CNCiLC (region I in Figure 3a) differs from that of CNCiiLC (regions II and III in Figure 3b). The top LC phase presents anisotropic and isotropic domains ( $\approx 2\text{--}10\ \mu\text{m}$  in length), forming interconnected domains evidenced by the pink and blue domains observed when the

lambda plate is inserted at  $45^\circ$  between the crossed polarizers. In CNCiiLC suspensions, tactoids with diameters of  $\approx 50\ \mu\text{m}$  are dispersed in the isotropic phase, which form the high-density LC phase after coalescence and sedimentation (Figure 3b1,b3 and b2,b4, regions II to III). The fingerprint texture within the tactoids reveals the existence of a cholesteric phase, which is well known to develop in CNC aqueous suspensions derived from filter paper,<sup>[16]</sup> bacteria,<sup>[32]</sup> and wood pulp.<sup>[12]</sup> Furthermore, the samples collected from the CNCiLC suspension (region A in Figure 3a) were observed between crossed polarizers and between crossed polarizers and a lambda plate, as shown in Figure 3a3,a4, respectively. The microscopic preparations show isotropic spindle-like domains (atactoids) of different sizes in a birefringent medium. Tactoids with characteristic fingerprint textures are not observed.

### 2.2.3. $^1\text{H}$ NMR Relaxometry

Besides the macroscopic and microscopic qualitative observations,  $^1\text{H}$  spin-lattice relaxation time ( $T_1$ ) measurements were performed to probe the dynamic behavior of water in CNCiLC and CNCiiLC aqueous suspensions.

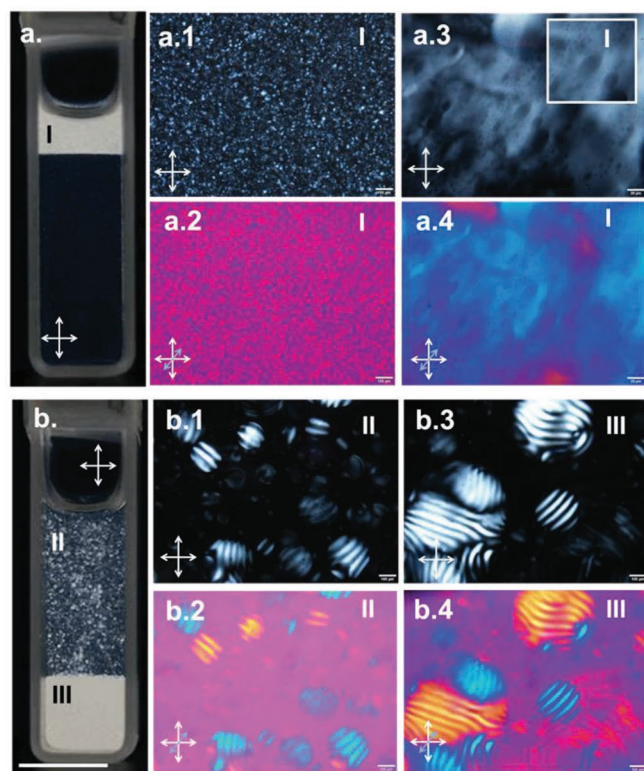


**Figure 3.** LC upper- and bottom-phases in CNC water suspensions. a,b) Vials with CNC colloidal suspensions of CNCi ( $C = 1.5\%$  w/w of CNCs in water) (region I: upper LC phase (CNCiLC)) (a) and CNCii (region II: middle (tactoids) and region III: bottom LC phase (CNCiiLC)) (b). a1,a2) Images from region I in (a) with small ( $2\text{--}10\ \mu\text{m}$ ) isotropic domains dispersed in an anisotropic medium. b1,b2) Images from region II in (b) showing anisotropic domains (tactoids) in an isotropic medium of different sizes with fingerprint texture. b3,b4) Images from region III marked in (b) showing the coalescence of tactoids. The samples in (a1), (a2), and (b1)–(b4) are confined in flat capillaries. a3,a4) Observation of a droplet on a microscope slide, collected from region I in (a) showing isotropic domains dispersed in a birefringent phase (spindle-like isotropic regions, zoomed in (a3)). All the samples are observed in the transmission mode. The images in (a1), (a3), (b1), and (b3) are captured between crossed polarizers, whereas those in (a2), (a4), (b2), and (b4) are captured between crossed polarizers with a lambda plate. c) Spin-lattice relaxation rate dispersions for CNCiLC and CNCiiLC suspensions compared to pure (bulk) water at  $25^\circ\text{C}$ . The scale bar in (b) (vial with the same dimensions as in (a)) is 1 cm.



The observed spin-lattice relaxation rate data for the CNCiLC and CNCiiLC samples are presented in Figure 3c. The spin-lattice relaxation data of bulk water are also depicted for comparison. Adding a component to water is expected to reduce the mobility compared to that of pure water, and this effect is highly sensitive to the amount, dimension, and chemical nature of the added component(s). However, it is noteworthy that in Figure 3c, the nuclear magnetic relaxation dispersion profiles of the CNCiiLC and CNCiLC suspensions are different. While the profile of the CNCiiLC suspension is almost identical to that of bulk water, the CNCiLC suspension relaxation rate is always lower. This implies that the water dynamics/mobility differs in the high- and low-density LC phases and is almost the same in the CNCiiLC aqueous suspension.

### 2.3. CNC Characterization

To further investigate the origin of the anisotropic low-density LC phase, CNCs were isolated from the CNCi and CNCii LC phases (CNCiLC and CNCiiLC) and isotropic phases (CNCii and CNCiil) and observed using AFM. The representative images of CNCiLC and CNCii are displayed in Figure 4a,b, while those of CNCiiLC and CNCiil are displayed in the Supporting Information (Figure S4 and Table S2, Supporting

Information). Analysis of the images reveals minor shape differences between the CNCs isolated from CNCi and CNCii (Figure 4c–e). The average length, diameter, and axial ratio of the CNCs were determined by the 250 considered nanorods, and the data were analyzed according to Honorato-Rios et al.<sup>[30]</sup> The average lengths of the CNCs from CNCiLC and CNCii are  $L_{iLC} = (204 \pm 78)$  nm and  $L_{ii} = (197 \pm 63)$  nm, respectively. CNCiLC is slightly more polydisperse than CNCii, with length polydispersities of 0.38 and 0.32 (ratio of standard deviation to average length), respectively. The average rod diameters of the CNCs from CNCiLC and CNCii are  $D_{iLC} = (5 \pm 1)$  nm and  $D_{ii} = (6 \pm 2)$  nm, respectively. The diameter polydispersity is similar for the CNCiLC (0.23) and CNCii (0.29) particles. The average values of the length and diameter of the CNCiLC and CNCii particles are similar. The average aspect ratio (calculated as the average of  $L/D$  for 250 single rods, according to Honorato-Rios et al.<sup>[30]</sup>) is slightly higher for the particles isolated from the CNCiLC phase ( $(L/D)_{iLC} = 45 \pm 19$  and  $(L/D)_{ii} = 38 \pm 16$ ). The AFM results show small differences between the particles isolated from the low-LC and the high-density isotropic phases; both show particles with similar average lengths and slightly different aspect ratios. Particles with higher aspect ratios exhibit a tendency to accumulate in the LC phase as expected.<sup>[16]</sup> Considering the average values of the length ( $189 \pm 81$  and  $204 \pm 78$  nm for the CNCii and CNCi particles, respectively)

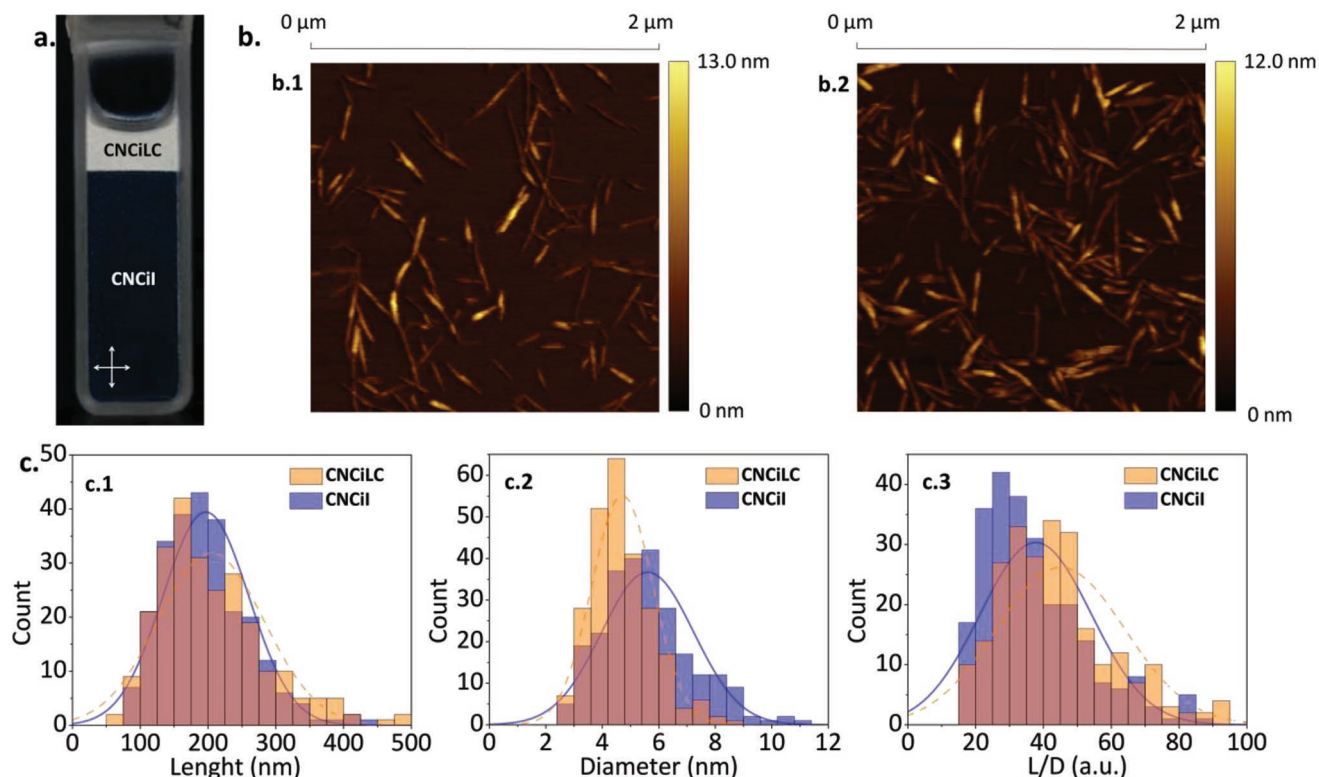


**Figure 4.** AFM images of the CNCs from the low-density LC and high-density isotropic phases. a) Image of the vial, between crossed polarizers, showing the anisotropic (upper phase CNCiLC) and isotropic (bottom CNCii phase) suspensions from which the nanoparticles are collected. b) AFM images of the nanoparticles collected from the CNCii (left image) and CNCiLC (right image) phases. c) Distribution of the length ( $L$ ), width ( $D$ ), and aspect ratio ( $L/D$ ) of the particles, from (c1) to (c3), respectively. The dashed orange line denotes CNCiLC particles and the blue curve denotes CNCii particles. On an average, particles with a higher axial ratio show a slight tendency to be in the CNCiLC phase, compared to the particles accumulated in the CNCii phase, as also shown in Table S2 (Supporting Information). The values of  $D$  and  $L$  are calculated as the average of 250 single rods.

and diameter (in the order of  $5 \pm 2$  nm for both samples), the particle shape does not offer a reasonable explanation for the distinct phase separation and phase inversion observed in the suspensions prepared from the CNCii and CNCi samples.

The XRD pattern of CNCi particles show small differences compared with that of CNCii particles (Figure S5, Supporting Information). Both XRD patterns display characteristic peaks of cellulose nanocrystals at  $2\theta = 15.0^\circ$ ,  $16.0^\circ$ , and  $22.5^\circ$ , which correspond to the (101), (10 $\bar{1}$ ), and (002) crystallographic planes.<sup>[35]</sup> The crystallinity of the samples is also similar (86.7 for CNCi and 86.2 for CNCii).

The sulfur content in CNCi and CNCii was determined through elemental analysis for the isotropic and anisotropic phases. The sulfur content in the CNCiLC particles is 0.52%, which is lesser than that in the CNCiiLC particles (0.71%). This difference between the CNCiLC and CNCiiLC samples can be justified by the amount of water present in the never-dried sample, which inhibits esterification reaction with sulfuric acid.<sup>[36]</sup>

## 2.4. Solid Films

### 2.4.1. ATR-FTIR Spectra

To investigate the interaction of water with cellulose in sample (i) (“never-dried” pulp fibers) and sample (ii) (dried-pulp fibers), the attenuated total reflection Fourier-transform infrared spectroscopy (ATR-FTIR) spectra were acquired (Figure S6, Supporting Information). The more interesting and clearly visible

changes between the two spectra are related to the development of intra- and intermolecular hydrogen bonds at  $3445\text{ cm}^{-1}$  and water adsorption at  $1640\text{ cm}^{-1}$ . As expected, the O–H band is more intense for the “never-dried” sample (i). The crucial difference is the band at  $1640\text{ cm}^{-1}$  that appears for sample (i) but is not present in the spectrum of sample (ii). This band is assigned to the water present in the never-dried sample.<sup>[37]</sup>

In addition, the ATR-FTIR spectra of the dried samples obtained from the CNCi and CNCii suspensions were acquired (Figure S7, Supporting Information). The two spectra are similar. The presence of sulfate groups resulting from acid hydrolysis is revealed by the band at  $\approx 810\text{ cm}^{-1}$ , which can be assigned to S–O stretching.<sup>[38]</sup>

To further investigate the CNCi sample, the ATR-FTIR spectra of dried samples collected from the CNCi and CNCiLC phases were recorded (Figure S8, Supporting Information). These spectra are also similar. Bands at  $810\text{ cm}^{-1}$  due to S–O stretching are present in both samples.<sup>[39,40]</sup> These results indicate that sulfate groups are in the particles present in the isotropic and LC phases.

### 2.4.2. Scanning Electron Microscopy Characterization

The CNCiLC suspensions were freeze dried, and solid films were obtained using casting and observed using SEM (Figure 5a–c and Figure S9, Supporting Information). The cross-sections of the dried solid films from the CNCiLC and CNCiiLC phases were also observed using SEM (Figure 5c,d).

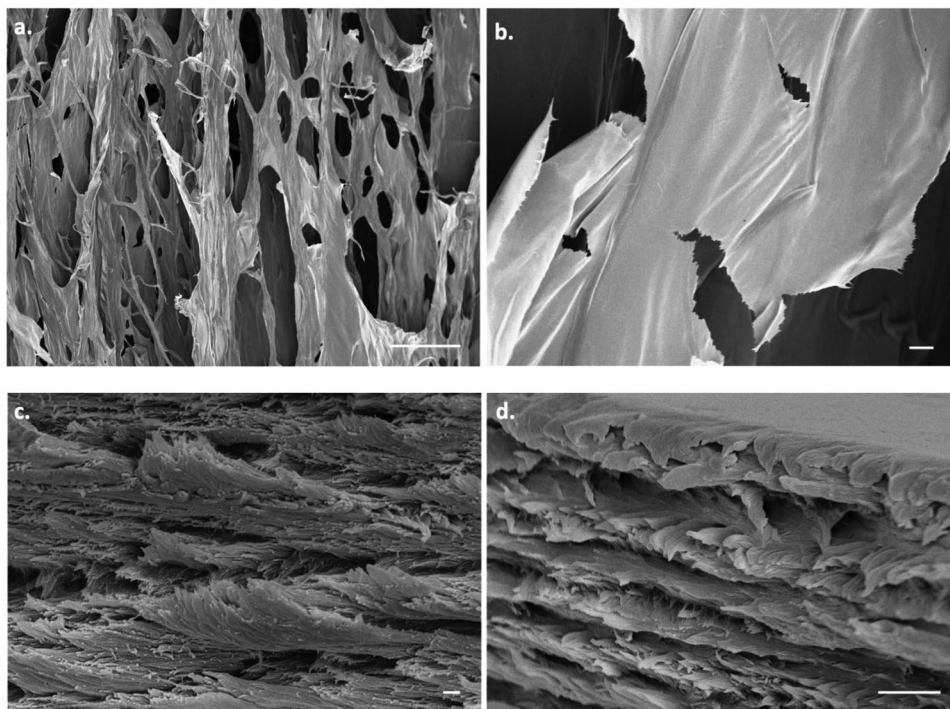


**Figure 5.** Solid samples from CNC colloidal liquid crystal phases: a,b) SEM images obtained from the low-density anisotropic phase colloidal suspensions prepared from CNCiLC suspension, after freeze drying. The “holes” in (a) and (b) resemble the isotropic spindle-like domains observed through POM (Figure 3a3,a4). The thickness of the sheet shown in (b) is 30 nm (see Figure S9, Supporting Information). c,d) Solid films prepared from dried droplets of CNCiLC and CNCiiLC colloidal suspensions, respectively. A layered structure is observed in both samples. The scale bars for (a)–(d) are 100  $\mu\text{m}$ , 2  $\mu\text{m}$ , 200 nm, and 1  $\mu\text{m}$ , respectively.

The freeze-dried CNCiLC sample reveals the existence of crumpled torn leaves (thickness in the order of 30 nm), with “holes” of different sizes (Figure 5a,b). The “hole” shape is similar to that of the atactoids observed using POM (Figure 3a3,a4), suggesting that the atactoids in the anisotropic suspension are held in the solid freeze-dried nanosheets.

The cross-sections of the dried films from the CNCiLC and CNCiILC suspensions indicate the formation of a layered structure for both LC samples upon the slow evaporation of water. The cross-section of the film obtained from the CNCiILC sample shows particles aligned in a cholesteric structure, as previously reported and studied, with an average helical pitch of  $0.56 \pm 0.05 \mu\text{m}$ . This cross-section is different than that of the dried film obtained from the CNCiLC suspension where the pitch cannot be determined in the visible range.

#### 2.4.3. X-ray Photoelectron Spectroscopy and Wettability Measurements

To further investigate the CNCi and CNCii suspensions, solid films were prepared from the CNCiLC, CNCiILC and CNCiI, and CNCiIL phases and characterized using XPS and wettability measurements.

For the CNCiI and CNCiLC films, the XPS survey profiles (Figure 6a) reveal the existence of C 1s, O 1s, and S 2p signals with binding energies (BEs) of  $\approx 286$ , 533, and 169 eV, respectively (similar to that observed in the spectra of CNCiIL and CNCiILC films (see Figures S10 and S11 and Tables S3 and S4, Supporting Information)). The atomic (%) of C, O, and S are 61.7%, 37.8%, and 0.48%, respectively, for the CNCiI films and 58.9%, 40.6%, and 0.52% for the CNCiLC samples, respectively (see Table S3, Supporting Information and

Belgacem et al.<sup>[41]</sup>) The oxygen-to-carbon ratio (O/C) for the CNCiI samples (0.61) is lesser than that for CNCiLC (0.69); the latter is similar to that of neat CNCiILC (0.69). More evident differences are found in the films obtained from the isotropic phases in which the oxygen-to-carbon ratio (O/C) is lesser (0.61) for CNCiI and higher (0.71) for CNCiIL, compared to those of the films obtained from CNCiLC and CNCiILC, respectively. The films from CNCiLC and CNCiILC present similar spectra in the region of the C 1s spectra (Figure 6b). Deconvolution of these core spectra shows the contribution of four component peaks. The CNCiLC, CNCiILC, CNCiI, and CNCiIL C 1s core spectra exhibit a similar main peak at 286.6 eV attributed to the C—O—H and C—O—C bonds (Table S4, Supporting Information). However, for the CNCiI films, the contribution of the peak at 284.8 eV, assigned to the C—H and C—C bonds, is higher than those observed in the CNCiLC, CNCiIL, and CNCiILC films. Moreover, the contribution of the peak at 288 eV, ascribed to C=O and O—C—O, increases for CNCiLC compared to the same deconvoluted peak observed for CNCiILC (Figure 6b and Table S3, Supporting Information). These observations can indicate that the hydrophilic hydroxyl groups, bonded equatorially to the glucopyranose ring of cellulose, are arranged with a slight difference in the CNCiLC and CNCiILC films. The peak at 289 eV, associated with the O—C=O groups, is residual in both spectra. To further investigate the solid films, water contact angle (CA) measurements were performed.

The surface characterization of the CNCiLC and CNCiILC films (Figure 6c,d) using CA measurements was not easy due to the absorbent nature of the film surfaces. However, a rough estimation of the surface properties was made through CA measurements. The CNCiLC film surface exhibits a clear tendency to be more hydrophilic ( $\text{CA} = 31^\circ \pm 2^\circ$ ;  $n = 7$ ) than the CNCiILC film ( $\text{CA} = 48^\circ \pm 2^\circ$ ;  $n = 7$ ).

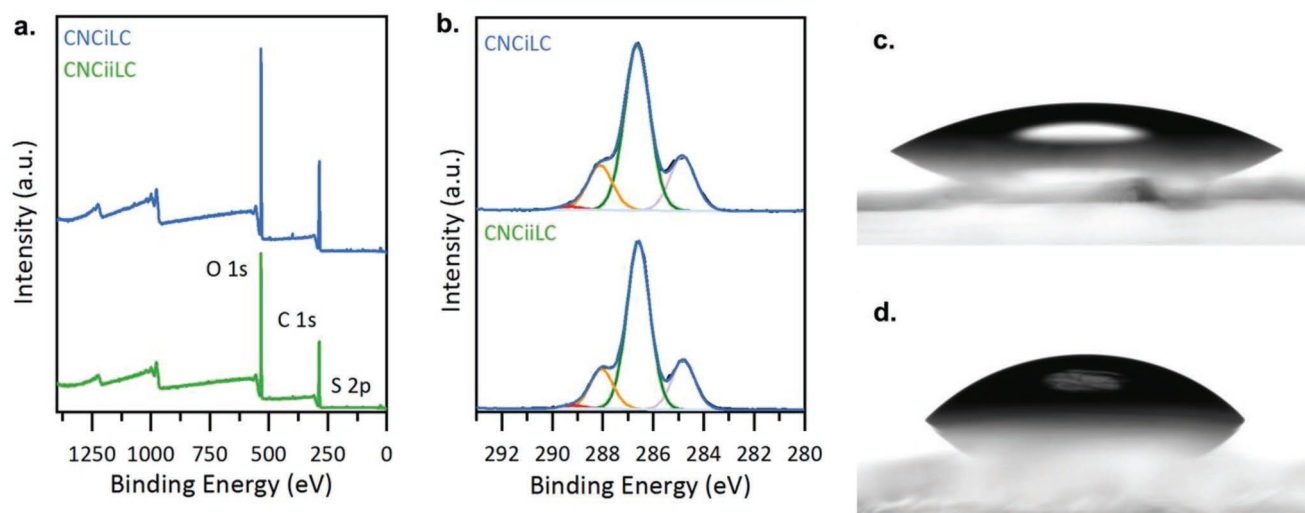


**Figure 6.** Solid-film XPS and wettability measurements. a) Wide-scan XPS survey spectrum of the solid films prepared from CNCiLC and CNCiILC suspensions, showing the presence of sulfur in all the films. b) Core level C 1s XPS spectra and the respective deconvoluted peaks for the CNCiLC and CNCiILC solid films. The contributions of the peaks from C—H and C—C are similar for the CNCiLC and CNCiILC solid films, whereas the area of the peaks assigned to O—C—O and C=O and C—O—H and C—O—C shows a small tendency to increase for the CNCiILC film. c) Water droplet on the more hydrophilic CNCiLC surface and d) on the less hydrophilic CNCiILC surface.



### 3. Discussion

We demonstrated that polydisperse CNC aqueous suspensions above a critical concentration could separate into a low-density LC (CNCiLC) phase co-existing with an isotropic (CNCii) high-density phase. Phase inversion was only observed if the suspensions were prepared from CNCi particles isolated from never-dried *eucalyptus* kraft pulp, and the CNCi suspensions were freeze–thawed after acid hydrolysis and before dialysis. The same procedure was applied for isolating CNCs from dried *eucalyptus* kraft pulp, re-hydrated pulp, and wet cotton. Aqueous suspensions prepared using the CNCs isolated from these sources showed a separation between the high-density LC phase and low-density isotropic phase, in accordance with literature.<sup>[16]</sup> If suspensions with a low-density LC phase (CNCiLC) were mixed with high-density LC suspensions (e.g., CNCiiLC) with the same CNC concentration (1.5% w/w), the colloidal suspensions separated into an isotropic bottom phase co-existing with a low-density LC phase, similar to CNCiLC suspensions (Figure S1, Supporting Information). This indicates that the observed anomalous effect can be induced in high-density CNC LC phases.

It is noteworthy that the CNCs isolated from isotropic and low- and high-density LC phases have similar average diameters and lengths after drying, indicating that sample polydispersity is not the cause for the development of the low-density LC phase. However, the solid particles isolated from the low- and high-density LC phases give rise to solid films with surfaces that are slightly more hydrophilic when prepared from particles isolated from low-density LC phases.

POM and <sup>1</sup>H NMR relaxometry revealed the main differences between the high- and low-density LC suspensions. Through POM, isotropic spindle-like domains could be observed in the low-density LC phase contrasting with the well-known existence of tactoids in the high-density LC phase. <sup>1</sup>H spin-lattice relaxation time measurements indicated that the interaction of the low- and high-density anisotropic phases with water were different. This can be explained by the lower hydrophilicity of the CNCiiLC particles compared to the CNCiLC particles. Therefore, very few water molecules interacted with the CNCiiLC particles, and a water-like dispersion was observed. On the contrary, the relaxation rate for the CNCiLC sample exhibited a similar frequency dependence but systematically lower values compared to the CNCiiLC sample. The lower relaxation rate in the CNCiLC-based suspension is presumably due to the enhanced hydrophilic character of the CNCiLC particles, suggesting relatively stronger interaction between the water molecules and CNCiLC particles.

In a suspension, the difference between the high- and low-density phases is clear. However, as previously mentioned, the dried CNCs collected from the high- and low-density phases are similar in length and diameter. If the low-density phase is separated from the isotropic phase and subsequently re-diluted with water, the isotropic phase remains a high-density phase. Furthermore, the mass fraction of CNCi particles is higher in the low-density phase than in the high-density one. These data suggest that the existence of the low-density phase cannot be justified by the particle polydispersity for suspensions of platelike colloids.<sup>[2,3]</sup>

A crucial factor for the existence of the low-density LC phase is associated with the usage of a never-dried sample. Never-dried

*eucalyptus* kraft pulp presents a considerably different IR spectrum compared to those of the other sources used in this study. IR spectra evidence the presence of water in the never-dried sample. Different types of water interactions with cellulose have been described in literature.<sup>[42]</sup> Recently, it has been reported that the presence of water influences the reactivity of cellulose as well.<sup>[36]</sup> It is known that cellulose is an amphiphilic macromolecule that can self-adapt its conformation with the environment.<sup>[43,44]</sup> While the spectra of the starting materials reveal the presence of cellulose fibers and water, the CNCs isolated from CNCi and CNCii suspensions show similar IR spectra, indicating that both dried particles have a similar chemical composition. However, the surfaces of the solid films produced from CNCiLC and CNCiiLC exhibit different hydrophilicity values as shown by the wettability measurements. These findings appear to corroborate the results obtained through <sup>1</sup>H NMR relaxometry that the particles from high- and low-density LC phases interact differently with water.

Not only is the presence of water important in the never-dried sample, but FT is also expected to play a role in the observed phenomena. To confirm this, CNCs were obtained from the same never-dried sample following a procedure that did not include freeze–thawing the suspensions before dialysis. In this case, the LC phase does not separate from the isotropic phase, confirming that freeze–thawing is also crucial for the development of the low-density LC phase.

As the suspensions prepared from the re-hydrated samples and hydrated cotton show a high-density LC phase, the water in the never-dried sample is expected to be present not only on the surface but also within the fibers. The CNC source appears crucial for the existence of entrapped water. The plant determines these interactions, and our results indicate that after the water is removed, it cannot re-enter the structure. Moreover, water can dissolve a certain volume of air (1000 mL of water at 0 °C can dissolve ≈30 mL of air); therefore, when water solidifies into ice, the air escapes out, forming bubbles in solid ice.<sup>[45]</sup>

A possible hypothesis to interpret the obtained results involves the assumption that the dispersed nanocellulose and air are expelled from the growing ice crystals when the suspensions are frozen. If water is present within the nanoparticles, its crystallization into ice separates from the CNCs and air. Wettability measurements indicate a slightly change in the cellulose conformation, which can be attributed to the presence of air in the cellulose phase of the frozen suspensions. This modification of the conformation should allow capture of air in the CNCs. When cellulose fibers are dried in air, the fiber structure changes and it is difficult to revert to the initial conformation of cellulose (“hornification”).<sup>[46]</sup> A similar irreversible process can be at work when cellulose is dried in an ice environment. We suggest that the entrapped air within the CNCs is responsible for the low-density LC phase (Scheme SI, Supporting Information). Thereby, the LC phase is an indirect method for detecting the involvement of the CNC chains with water.

### 4. Experimental Section

**Cellulose Nanocrystal (CNC) Preparation and Colloidal Aqueous Suspensions:** CNCs were prepared according to a method described in literature<sup>[29]</sup> modified by the following: The acid hydrolysis of never-dried

BEKP (29% w/w water content), dried BEKP, re-hydrated BEKP (29% w/w water content), and wet cotton (35% w/w of water), (15 g of each sample) was performed with sulfuric acid (Sigma-Aldrich, 95–97%) diluted to 62% w/w with an acid solution/solid ratio of 8:1 for a duration of 75 min at 50 °C under mechanical stirring, followed by quenching with 10× ultrapure water (Millipore Elix Advantage 3 system). The resultant materials were centrifuged with ultrapure water in consecutive cycles and the CNC suspensions were collected for pH values ranging from 1.9 to 3.9. The diluted suspensions ( $\approx 3$  L) were freeze-thawed ( $-15$  °C) to reduce the volume prior to dialysis. A batch of diluted suspensions of the CNCs obtained from never-dried BEKP (29% w/w water content) was not freeze-thawed prior to dialysis. The product was dialyzed (Spectra/Por 4 membrane, molecular cut-off 12–14 kDa) against ultrapure water for at least 3 weeks until pH became constant. The diluted CNC suspensions were vacuum-filtered and concentrated with an osmotic bath using poly(ethylene glycol) (PEG), based on the method described by Frka-Petecic et al.<sup>[47]</sup> The samples were placed in a dialysis membrane (SnakeSkinTM tubing, Thermo-Fisher, molecular weight cut-off of 3.5 kDa), which was immersed in an aqueous solution of 20% w/w PEG (Sigma-Aldrich, 35 kDa), and under magnetic stirring until  $\approx 10\%$  of the initial volume was attained. The concentrated suspensions with CNCs ( $\approx 100$  mL) were treated with 10 min of sonication (the sonication tip pulsed at an output power of 360 W with 100% amplitude level and a 0.8 cycle) over an ice bath, using a UP400 S ultrasonic processor (400 W, 24 kHz, Hielscher Ultrasonics GmbH). The suspensions with CNC content ranging from 3.5 to 6.5% w/w (gravimetrically determined) were used in an acidic form (pH = 3.5).

**Phase Diagrams:** Phase diagrams were obtained from the CNC suspensions diluted to 2.5–6.5% w/w (source dependent) to yield 10 mL samples, which were sonicated (output power of 360 W with 100% amplitude level and a 0.8 cycle) thrice within 5–10 min (depending on the temperature and initial concentration). For each batch, the sonicated mother suspensions were diluted into samples with the CNC content ranging from 1.1 to 2.5% w/w (CNCi, ii and iii) and 4.0–6.5% w/w (CNCiv). The samples were allowed to separate into isotropic and anisotropic phases, and were photographed between crossed polarizers. The anisotropic fraction value for each sample was the average of six measurements, and the error bar was considered as the standard deviation of all the measurements (using ImageJ software, Version 1.52a, <https://imagej.nih.gov/ij/><sup>[48]</sup>). A freeze drier (Zirbus GmbH Vaco 2-E) was used to obtain freeze-dried samples of the upper LC phases used for SEM.

**Polarized Optical Microscopy:** Using a microscope (Olympus BX51) coupled with a CCD camera (Olympus DP73) and using the Stream Basic v.1.9 Olympus software, images were obtained in the transmission mode. A halogen lamp (KL 2500 LCD, SCHOTT) was employed as the cold illumination source. The images were obtained with an objective of  $\times 10$ ,  $\times 20$ , or  $\times 50$  (Olympus, MPlanFL N) and automatically scaled by the software.

**$^1\text{H}$  NMR Relaxometry:**  $^1\text{H}$  spin-lattice relaxation time ( $T_1$ ) measurements for investigating the water dynamics in the CNCiLC and CNCiiLC samples were performed at 25 °C across a frequency range of 15–300 MHz. A Bruker 7T superconducting magnet with a Bruker Avance II NMR console and a variable-field (0.2–2 T) iron core electromagnet (BE30), also connected to the same console, were employed for measuring the  $T_1$  values. During these NMR measurements, a standard airflow system controlled the temperature with a precision of  $\pm 0.5$  °C. The experimental error of the spin-lattice relaxation time measurements was estimated to be  $\approx 5\%$ . The time evolution of longitudinal magnetization was acquired with 32 distinct values of the variable delay time  $t$ , and in order to determine the  $T_1$  values at each frequency, was fitted to a mono-exponential recovery function

$$M_z(t) = M_z^\infty + (M_z^0 - M_z^\infty)e^{-t/T_1} \quad (1)$$

The above equation indicates that the z-magnetization  $M_z(t)$  returns from the perturbed state  $M_z^0$  to the equilibrium state  $M_z^\infty$  following an exponential law.

**Mass Fraction Measurements:** The CNC amount in % w/w for each fraction (anisotropic and isotropic) was determined through a gravimetric technique. To determine the mass fraction, a Sartorius analytic scale (model Quintix224-1S, readability of 0.1 mg) was used. All the measurements were obtained in a controlled environment at  $20.0 \pm 0.1$  °C and  $57 \pm 1\%$  relative humidity. Regular calibration of the scale and micropipettes was performed as specified by the supplier, and tweezers were used to manipulate the samples. In general, for mass fraction determination, 50  $\mu\text{L}$  aliquots of the CNC suspension were placed in a 0.5 mL Eppendorf and the weight ( $w_1$ ) was determined. The suspension was allowed to dry at 60 °C until its weight ( $w_2$ ) became constant, i.e., until three consecutive weight readings at given time intervals were equal (within the readability value of the scale). The fraction value in percentage is given by the expression  $(w_2/w_1) \times 100$ .

The reported values for the mass fraction represented the mean and standard deviation of five replicas for each fraction, unless stated otherwise.

**Elemental Analysis:** A Horiba Jobin Yvon ULTIMA sequential ICP with a monochromator equipped with a Czerny Turner spectrometer and Horiba Jobin Yvon ICP Analyst 5.4 software was used to determine the sulfur content of the samples under argon. The samples (a known amount per mL) were immersed in nitric acid (PanReac AppliChem, 69%) at 100 °C until total digestion. The results were the average of two independent measurements; one significant digit was considered.

**Scanning Electron Microscopy:** SEM images of the freeze-fracture cross-sections of the films and those of the upper anisotropic phase of the freeze-dried samples were obtained using a Carl Zeiss Auriga crossbeam (SEM–focus-ion-beam) workstation instrument equipped with an Oxford energy-dispersive X-ray spectrometer. For freeze-fracture, the sample was fractured by immersion in liquid nitrogen until it was frozen and then struck to cause a fracture. The samples were mounted in aluminium stubs coated with a thin carbon layer using a Q150T ES Quorum sputter coater. Acquisition was performed at an accelerating voltage of 3 or 5 kV at a working distance of 6.5–7.2 mm.

**X-ray Photoelectron Spectroscopy:** Kratos Axis Supra equipment with a monochromatic Al K-alpha source (1486.6 eV) was used to acquire the XPS spectra at 15 kV under a current of 10 mA. All the spectra were recorded in detail at pass energies of 160 and 10 eV, for survey and detailed scans, respectively. An electron flood gun was used for charge neutralization during measurement; all the peaks were shifted to C 1s at 284.8 eV. CasaXPS Version 2.3.19PR1.0 software was used for data analysis. The relative sensitivity factors for quantification were provided by the manufacturer.

**Fourier-Transform Infrared (FTIR) Spectroscopy:** The FTIR spectra of the samples were recorded using a Perkin-Elmer FTIR Spectrometer Spectrum Two (Waltham, MA, USA) equipped with an ATR cell, in the range of 4000–500  $\text{cm}^{-1}$ . The dried and never-dried samples were placed directly on the ATR cell without further pretreatment.

**X-ray Diffraction:** The XRD patterns of the films were acquired with a diffractometer (PANalytical, model X'Pert Pro) using  $\text{CuK}\alpha$  line radiation ( $\lambda = 1.5406$  Å) at 45 kV and 40 mA in the  $5^\circ < 2\theta < 40^\circ$  angular range with a scanning step of  $0.05^\circ \text{ min}^{-1}$ .

The crystallinity index was calculated as follows<sup>[49]</sup>

$$I_{\text{cryst}} = \frac{I_{002} - I_{\text{am}}}{I_{002}} \quad (2)$$

where  $I_{\text{cryst}}$  is the crystallinity index,  $I_{002}$  is the peak intensity at the (002) plane at  $2\theta = 22.5^\circ$ , and  $I_{\text{am}}$  is the height of amorphous cellulose (minimum intensity at the valley between planes (002) and (110)).

**Photographs and Videos:** Photographs and videos of the suspensions in vials were captured with a Canon EOS 550D coupled with an EF-S 60 mm Canon macro-lens under an incandescent white ring light, obtained between crossed polarizers, unless stated otherwise.

**Atomic Force Microscopy:** For particle size distribution, the average length and width of the CNCs were determined from 250 measurements using Gwyddion software (version 2.52, <https://gwyddion.net/><sup>[50]</sup>), from the AFM images acquired with an Asylum Research MFP-3D standalone system in the tapping mode (Santa Barbara, CA, USA) with commercially

available silicon AFM probes at a scanning frequency of 300 kHz and  $k = 26 \text{ N m}^{-1}$ .

**Contact Angle (CA) Measurements:** An OCA20 CA measuring instrument (DataPhysics Instruments GmbH, Filderstadt, Germany) was used to determine the static water CAs on the sample surfaces using the sessile drop method. Samples were obtained by drying 100 mL droplets of CNC suspensions on a glass substrate until their weight was constant. Water droplets of 2  $\mu\text{L}$  were formed using an electronic micrometric syringe and deposited on the film substrate surface according to the so-called pick-up procedure. Image acquisition, analysis, and CA determination were performed using the SCA20 v.4.3.12 software (Dataphysics Instruments GmbH, Filderstadt, Germany). A total of seven droplets were dispensed, and each droplet was placed on a different region of the sample surface. Three different films were used for each measurement. The CAs were determined after 2 s of droplet deposition and settling. The results were corresponded to the average CA and were presented with the respective standard deviation.

**Statistical Analysis:** The quantitative data were presented as the mean, and the sample size was mentioned in the description of the adopted method. The error was estimated by calculating the standard deviation (SD) of the mean and was given as mean  $\pm$  SD.

## Supporting Information

Supporting Information is available from the Wiley Online Library or from the author.

## Acknowledgements

This work was co-financed by FEDER, European funds, through the COMPETE 2020 POCI and PORL, National Funds through FCT—Portuguese Foundation for Science and Technology and POR Lisboa2020 under projects PIDDAC (POCI-01-0145-FEDER-007688, Reference UIDB/50025/2020-2023), PTDC/CTM-REF/30529/2017 (NanoCell2SEC), Action European Topology Interdisciplinary Action (EUTOPIA CA17139), and Project Inpactus—innovative products and technologies from eucalyptus, Project no. 21874 funded by Portugal 2020 through European Regional Development Fund (ERDF) in the frame of COMPETE 2020 no. 246/AXIS II/2017.

## Conflict of Interest

The authors declare no conflict of interest.

## Author Contributions

M.H.G. supervised and directed this project. R.R.R. prepared the samples and performed XRD, FTIR, and elemental analysis. R.R.R. and M.H.G. performed SEM analysis. R.R.R., P.E.S.S., and M.H.G. performed time-lapse photography and POM. D.V.S. and R.R.R. performed AFM measurements. S.N.F. performed contact angle and XPS measurements. A.K. and P.S. performed  $^1\text{H}$  NMR relaxometry. A.P.M.S. supplied the *Eucalyptus* Kraft Pulps and contributed to their characterization. M.H.G. wrote the manuscript, and all the authors contributed to the improvement and editing of the paper.

## Data Availability Statement

The data that support the findings of this study are available from the corresponding author upon reasonable request.

## Keywords

aqueous suspensions, cellulose nanocrystals (CNCs), liquid crystals, low-density liquid crystalline phase

Received: October 14, 2021

Revised: April 28, 2022

Published online: June 6, 2022

- [1] L. Onsager, *Ann. N. Y. Acad. Sci.* **1949**, *51*, 627.
- [2] H. N. W. Lekkerkerker, P. Coulon, R. Van Der Haegen, R. Deblieck, *J. Chem. Phys.* **1984**, *80*, 3427.
- [3] G. J. Vroege, H. N. W. Lekkerkerker, *J. Phys. Chem.* **1993**, *97*, 3601.
- [4] R. H. Marchessault, F. F. Morehead, N. M. Walter, *Nature* **1959**, *184*, 632.
- [5] A. C. Neville, D. C. Gubb, R. M. Crawford, *Protoplasma* **1976**, *90*, 307.
- [6] S. Vignolini, P. J. Rudall, A. V. Rowland, A. Reed, E. Moyroud, R. B. Faden, J. J. Baumberg, B. J. Glover, U. Steiner, *Proc. Natl. Acad. Sci. USA* **2012**, *109*, 15712.
- [7] A. P. C. Almeida, J. P. Canejo, S. N. Fernandes, C. Echeverria, P. L. Almeida, M. H. Godinho, *Adv. Mater.* **2018**, *30*, 1703655.
- [8] M. Mitov, *Soft Matter* **2017**, *13*, 4176.
- [9] S. N. Fernandes, L. F. Lopes, M. H. Godinho, *Curr. Opin. Solid State Mater. Sci.* **2019**, *23*, 63.
- [10] A. C. Neville, S. Caveney, *Biol. Rev. Cambridge Philos. Soc.* **1969**, *44*, 531.
- [11] J. F. Revol, H. Bradford, J. Giasson, R. H. Marchessault, D. G. Gray, *Int. J. Biol. Macromol.* **1992**, *14*, 170.
- [12] S. Beck-Candanedo, M. Roman, D. G. Gray, *Biomacromolecules* **2005**, *6*, 1048.
- [13] G. Delepierre, S. Eyley, W. Thielemans, C. Weder, E. D. Cranston, J. O. Zoppe, *Nanoscale* **2020**, *12*, 17480.
- [14] F. Jiang, A. R. Esker, M. Roman, *Langmuir* **2010**, *26*, 17919.
- [15] L. Lewis, S. G. Hatzikiriakos, W. Y. Hamad, M. J. MacLachlan, *ACS Macro Lett.* **2019**, *8*, 486.
- [16] X. M. Dong, J. F. Revol, D. G. Gray, *Cellulose* **1998**, *5*, 19.
- [17] W. Y. Hamad, *Cellulose Nanocrystals: Properties, Production and Applications*, Wiley, New York **2017**.
- [18] D. V. Saraiva, R. Chagas, B. M. de Abreu, C. N. Gouveia, P. E. S. Silva, M. H. Godinho, S. N. Fernandes, *Crystals* **2020**, *10*, 122.
- [19] C. Schütz, J. R. Bruckner, C. Honorato-Rios, Z. Tosheva, M. Anyfantakis, J. P. F. Lagerwall, *Crystals* **2020**, *10*, 199.
- [20] P.-X. Wang, M. J. MacLachlan, *Philos. Trans. R. Soc., A* **2018**, *376*, 20170042.
- [21] A. P. Philipse, A. Verberkmoes, *Phys. A* **1997**, *235*, 186.
- [22] A. Stroobants, H. N. W. Lekkerkerker, T. Odijk, *Macromolecules* **1986**, *19*, 2232.
- [23] J. H. L. Watson, W. Heller, W. Wojtowicz, *Science* **1949**, *109*, 274.
- [24] F. C. Bawden, N. W. Pirie, J. D. Bernal, I. Fankuchen, *Nature* **1936**, *138*, 1051.
- [25] K. Coper, H. Freundlich, *Trans. Faraday Soc.* **1937**, *33*, 348.
- [26] P. W. Oakes, J. Viamontes, J. X. Tang, *Phys. Rev. E: Stat., Nonlinear, Soft Matter Phys.* **2007**, *75*, 61902.
- [27] F. M. van der Kooij, D. van der Beek, H. N. W. Lekkerkerker, *J. Phys. Chem. B* **2001**, *105*, 1696.
- [28] A. A. Verhoeff, H. H. Wensink, M. Vis, G. Jackson, H. N. W. Lekkerkerker, *J. Phys. Chem. B* **2009**, *113*, 13476.
- [29] L. Chen, Q. Wang, K. Hirth, C. Baez, U. P. Agarwal, *Cellulose* **2015**, *22*, 1753.
- [30] C. Honorato-Rios, C. Lehr, C. Schütz, R. Sanctuary, M. A. Osipov, J. Baller, J. P. F. Lagerwall, *NPG Asia Mater.* **2018**, *10*, 455.



- [31] E. D. Cranston, D. G. Gray, *Biomacromolecules* **2006**, 7, 2522.
- [32] A. Hirai, O. Inui, F. Horii, M. Tsuji, *Langmuir* **2009**, 25, 497.
- [33] J. P. F. Lagerwall, C. Schütz, M. Salajkova, J. Noh, J. H. Park, G. Scalia, L. Bergström, *NPG Asia Mater.* **2014**, 6, e80.
- [34] S. Beck, J. Bouchard, R. Berry, *Biomacromolecules* **2011**, 12, 167.
- [35] S. Park, J. O. Baker, M. E. Himmel, P. A. Parilla, D. K. Johnson, *Biotechnol. Biofuels* **2010**, 3, 10.
- [36] M. Beaumont, P. Jusner, N. Gierlinger, A. W. T. King, A. Potthast, O. J. Rojas, T. Rosenau, *Nat. Commun.* **2021**, 12, 2513.
- [37] S. Y. Oh, D. Il Yoo, Y. Shin, G. Seo, *Carbohydr. Res.* **2005**, 340, 417.
- [38] D. Gaspar, S. N. Fernandes, A. G. de Oliveira, J. G. Fernandes, P. Grey, R. V. Pontes, L. Pereira, R. Martins, M. H. Godinho, E. Fortunato, *Nanotechnology* **2014**, 25, 094008.
- [39] D. Klemm, F. Kramer, S. Moritz, T. Lindström, M. Ankerfors, D. Gray, A. Dorris, *Angew. Chem., Int. Ed.* **2011**, 50, 5438.
- [40] F. Xu, J. Yu, T. Tesso, F. Dowell, D. Wang, *Appl. Energy* **2013**, 104, 801.
- [41] M. N. Belgacem, G. Czeremuszkin, S. Sapieha, A. Gandini, *Cellulose* **1995**, 2, 145.
- [42] S. Cichosz, A. Masek, *Materials* **2020**, 13, 4573.
- [43] L. S. Johansson, T. Tammelin, J. M. Campbell, H. Setälä, M. Österberg, *Soft Matter* **2011**, 7, 10917.
- [44] P. E. S. Silva, R. Chagas, S. N. Fernandes, P. Pieranski, R. L. B. Selinger, M. H. Godinho, *Commun. Mater.* **2021**, 2, 79.
- [45] N. Maeno, *Phys. Snow Ice, Proc.* **1967**, 1, 207.
- [46] L. Salmén, J. S. Stevanic, *Cellulose* **2018**, 25, 6333.
- [47] B. Frka-Petescic, G. Guidetti, G. Kamita, S. Vignolini, *Adv. Mater.* **2017**, 29, 1701469.
- [48] C. A. Schneider, W. S. Rasband, K. W. Eliceiri, *Nat. Methods* **2012**, 9, 671.
- [49] Y. H. P. Zhang, L. R. Lynd, *Biotechnol. Bioeng.* **2004**, 88, 797.
- [50] D. Nečas, P. Klapetek, *Cent. Eur. J. Phys.* **2012**, 10, 181.